Stochastic Simulation of Hemagglutinin-Mediated Fusion Pore Formation

Susanne Schreiber,* Kai Ludwig,* Andreas Herrmann,* and Hermann-Georg Holzhütter[†]

*Humboldt-Universität zu Berlin, Mathematisch-Naturwissenschaftliche Fakultät I, Institut für Biologie/Biophysik, D-10115 Berlin, and [†]Humboldt-Universität zu Berlin, Charite, Bereich Medizin, Institut für Biochemie, D-10117 Berlin, Germany

ABSTRACT   Studies on fusion between cell pairs have provided evidence that opening and subsequent dilation of a fusion pore are stochastic events. Therefore, adequate modeling of fusion pore formation requires a stochastic approach. Here we present stochastic simulations of hemagglutinin (HA)-mediated fusion pore formation between HA-expressing cells and erythrocytes based on numerical solutions of a master equation. The following elementary processes are taken into account: 1) lateral diffusion of HA-trimers and receptors, 2) aggregation of HA-trimers to immobilized clusters, 3) reversible formation of HA-receptor contacts, and 4) irreversible conversion of HA-receptor contacts into stable links between HA and the target membrane. The contact sites between fusing cells are modeled as superimposed square lattices. The model simulates well the statistical distribution of time delays measured for the various intermediates of fusion pore formation between cell-cell fusion complexes. In particular, these are the formation of small ion-permissive and subsequent lipid-permissive fusion pores detected experimentally (R. Blumenthal, D. P. Sarkar, S. Durell, D. E. Howard, and S. J. Morris, 1996, *J. Cell Biol.* 135:63–71). Moreover, by averaging the simulated individual stochastic time courses across a larger population of cell-cell-complexes the model also provides a reasonable description of kinetic measurements on lipid mixing in cell suspensions (T. Danieli, S. L. Pelletier, Y. I. Henis, and J. M. White, 1996, *J. Cell Biol.* 133:559–569).

INTRODUCTION

Fusion of enveloped viruses with either the plasma membrane or the endosomal membrane of host cells is mediated by specific viral transmembrane proteins. To this end, the ectodomain of these spike proteins has to undergo a conformational change into a fusion-active structure. Spike proteins of enveloped viruses taken up into a host cell by the endocytic route (as, for example, the hemagglutinin (HA) of influenza virus, the G-protein (VSV-G) of vesicular stomatitis virus, or the E1/E2-protein of Semliki Forest virus) undergo a conformational change at the acidic pH milieu in the late endosomal lumen. For spike proteins of viruses fusing with the plasma membrane of a host cell at neutral pH, e.g., the Sendai virus (F protein) or the human immunodeficiency virus (HIV) (gp41/120 protein), the trigger is thought to be set by interaction between the spike protein and receptors of the plasma membrane. Despite differences in the molecular architecture of the spike proteins, the natural target membranes, the uptake mechanism for the virus, and the trigger for the respective conformational change, it is generally believed that essential features of the fusion process are conserved among the various enveloped viruses. A general scheme of the fusion process has to envisage the following main steps. 1) The virus binds to the respective receptors of its target membrane. Often, and rather typically, binding and fusion activity are implemented in the same viral protein (e.g., HA, VSV-G, or gp41/120). 2) A fusion-active conformation of the viral fusion protein is triggered. Interaction with the receptor of the target cell may be essential for this conformational change and the conformation itself. Similar motifs of the secondary and higher structure of the ectodomain of different spike proteins have been identified under conditions where fusion is mediated. Several studies suggest that the structural feature of an extended, triple-stranded rod-shaped α-helical coiled coil represents a common structural and functional motif of fusion proteins of various enveloped viruses (Skehel and Wiley, 1998) such as orthomyxoviruses (Carr and Kim, 1993; Bullough et al., 1994), paramyxovirus (Baker et al., 1999), retroviruses (Chan et al., 1997; Tan et al., 1997; Weissenhorn et al., 1997; Fass et al., 1996; Kobe et al., 1999; Caffrey et al., 1998), and filovirus (Weissenhorn et al., 1998; Malashkevich et al., 1999). The transition into a fusion-active structure is accompanied by the exposure of a hydrophobic fusion sequence inserting eventually into the target membrane (Durell et al., 1997). 3) A fusion pore is formed. Studies on influenza virus A (Morris et al., 1989; Ellens et al., 1990; Doms and Helenius, 1986; Danieli et al., 1996; Blumenthal et al., 1996) and baculovirus (Markovic et al., 1998) implicated that aggregation of the fusion proteins to a multimeric complex is required to form a fusion pore. Typically, to elucidate the intermediates of fusion pore genesis and their structures, fusion between viral-protein-expressing cells and appropriate target cells (e.g., red blood cells) is studied. Such a model system even allows detection of single fusion events between of two fusing cells.

Mathematical models may provide a powerful tool to simulate the fusion process, in particular between fusing cells, on a quantitative level and, by that, to understand common structural motifs and mechanisms of enveloped

virus fusion (Bentz, 2000, 1992; Ludwig et al., 1995). Recently, employing a mass action kinetic model, the dynamics and size of the multimeric fusion HA complex was studied by comparing computed and measured fractions of cells equipped with the first fusion pore (Bentz, 2000). However, the predictive power of existing models is limited by the fact that a reasonable but nevertheless phenomenological function was used for the statistical distribution of the various time-dependent pore-forming events across an ensemble of fusing cells. Danieli et al. (1996) applied a Hill equation to model the dependence of the time delay in the onset of the lipid flow ($\Delta\varphi$ signal) upon varying HA densities. Blumenthal et al. (1996) assumed that the time shift between occurrence of a change of the membrane potential of the target membrane ($\Delta\psi$ signal) and of the $\Delta\varphi$ signal in single-cell fusion measurements follows an exponential probability distribution. Similarly, Bentz (2000) postulated a binomial distribution of first fusion pores across the population of cell-cell fusion complexes studied. Evidently, the fitted value of model parameters, e.g., the minimum number of aggregated HA trimers required to form a nascent fusion site, is strongly influenced by the choice of the statistical distribution function. Therefore, we propose here a model approach that aims at predicting the statistical distribution of the various time-dependent stages in pore formation. The approach explicitly takes into account the stochastic nature of the various elementary processes underlying the fusion process on the level of individual cell-cell contacts: the size of the contact area between two fusing cells, the lateral movement of fusion proteins and receptor molecules in the respective bilayer, and the interactions between fusion proteins and receptors.

Our approach does not allow only simulation of single cell-cell fusion events but also fusion measurements performed on cell suspension. The observed fusion kinetics measured in a cell suspension by monitoring time-dependent changes in the flow of fluorescent lipids results from the superposition of the stochastic cell-cell fusion signals. Accordingly, our modeling approach consists of two steps: 1) stochastic simulation of the fusion process taking place between single cells and 2) simulation of fusion kinetics in cell suspensions by using the ensemble average of individual stochastic trajectories.

The chain of events leading to the formation of a fusion pore between individual cells defines a Markov process that is governed by a master equation. The numerical solution of the master equation is performed by the algorithm introduced by Gillespie (1976) and provides stochastic time courses for the distinct intermediates of single-cell fusion. Values for the three unknown rate constants of the model are chosen such that a satisfactory concordance is achieved between simulated and observed $\Delta\psi$ and $\Delta\varphi$ signals. Next, by averaging individual stochastic time courses across a sufficiently large number of cell-cell fusion complexes we demonstrate that the proposed model also provides a satis-

factory simulation of the fusion kinetics measured in cell populations.

MODEL

Simulation lattice

The initial step of fusion pore formation consists in the binding of a HA-expressing cell to the target cell. Upon binding, small contact sites are formed between the cells, where both cell membranes lie approximately parallel and sufficiently close to each other to enable molecular interactions between them. These contact sites constitute the effective contact area. For what follows it is important to remark that the effective contact area can be considerably smaller than the total contact area estimated from micrographs of fusing cells. For example, Kozlov and Chernomordik (1998) reported the effective contact area between fusing cells to amount to ~1 μm^2. On the other hand, the total contact area has been assumed to be on the order of ~30 μm^2 (Frolov et al., 2000). In the following, we restrict the stochastic simulations to the kinetic processes taking place within the effective contact area. To this end, both membrane regions involved in a contact site are represented as a two-dimensional lattice constituted by small squared membrane units (in the following referred to as unit cells) covering the membrane area (Fig. 1). The edge length of a unit cell is set to 6 nm, which corresponds approximately to the spatial extension of HA trimers (see Wilson et al., 1981; Böttcher et al., 1999). Diffusion of HA trimers and receptors is modeled by random transitions between adjacent cells of the simulation lattice. The lattice is considered continuous, so that molecules leaving at one side are reintroduced at the opposite side, thus keeping the number of molecules constant. Lateral movement of integral membrane proteins is mainly brought about by random collisions with membrane lipids. The mean jump distance for membrane lipids is ~0.8 nm (Träuble and Sackmann, 1972). Thus, modeling lateral diffusion by random transitions between lattice cells with edge length of 6 nm fulfills the prerequisite that the mean free path of the diffusing molecule has to be smaller than the characteristic length of the simulation lattice.

A single unit cell cannot be occupied by more than one molecule (HA or receptor R) in each of the respective membranes. The effective contact area is dissected into smaller simulation areas, each represented by a lattice of unit cells. As checked by successively increasing the size of the simulation lattice, 50 × 50 unit cells are enough to prevent a notable influence of marginal effects caused by re-entering fusion intermediates leaving the simulation lattice during the simulation. Although the simulation lattice was initially chosen for computational reasons, experimental data underline that this size is in good agreement with that of a single contact site.
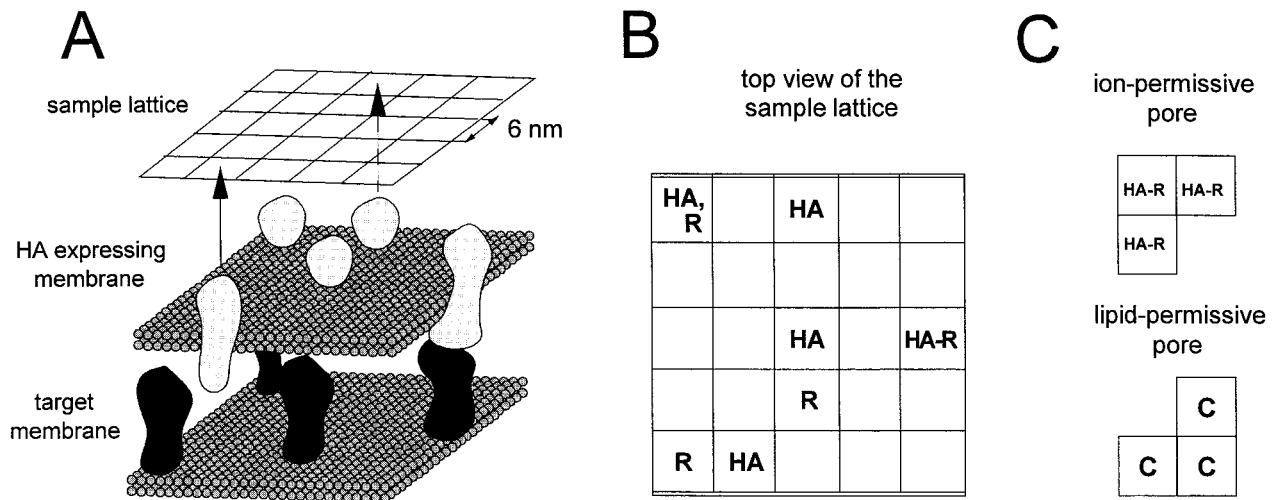
FIGURE 1 Definition of the simulation lattice. (*A*) The effective contact area between fusing cells is considered to be formed by a number of contact sites representing a certain area within the interface between the cells where the two membranes are arranged in parallel to each other and in a sufficiently close distance allowing the formation of HA-receptor contacts. The arrows illustrate how the various macromolecular structures involved in the fusion process are mapped onto the simulation lattice. (*B*) Occupation state of the simulation lattice derived from the constellation in *A*. Generally, a unit cell of the simulation lattice can be occupied by one of the following variables: R, receptor molecule, freely diffusing; HA, HA (trimer) molecule, freely diffusing; HA*, HA (trimer) molecule belonging to a HA cluster (immobile); HA-R, unstable HA-receptor contact (immobile); C, tight HA-receptor-membrane link (immobile). Note that one HA trimer and one receptor molecule can simultaneously occupy one unit cell because they are actually located in two different membrane planes. Furthermore, note that the smallest lattice in simulation was of 50×50 unit cells. (*C*) Definition of an ion-permissive pore ($\Delta\psi$ signal) and a lipid-permissive pore ($\Delta\varphi$ signal).

The cumulative distribution function $F_{tot}(t)$ for any fusion intermediate to occur within the time span t in the effective contact area between two fusing cells can be related to the corresponding distribution function $F_{sample}(t)$ for a simulation lattice by

$$F_{tot}(t) = 1 - [1 - F_{sample}(t)]^N, \qquad (1)$$

where N refers to the number of simulation lattices required to cover the effective contact area. Equation 1 can be easily rationalized by considering that $p = 1 - F_{sample}(t)$ is the probability that a fusion intermediate has not occurred within time span t in a single simulation area. Hence, the probability that this intermediate has not occurred within this time span in any of the N independent simulation areas is given by p^N.

Following Kozlov and Chernomordik (1998), the total contact area between fusing cells amounts to ~ 1 μm^2. Based on this value, the distribution function (Eq. 1) has to be calculated from the distribution function of $N = 12$ (12×0.09 $\mu m^2 \approx 1$ μm^2) simulation lattices.

Model variables and processes

The variables of the fusion model and the elementary processes that may take place between them are detailed in the following.

HA: activated hemagglutinin trimers

HA is organized as a homotrimer in the membrane. Each monomer consists of two disulfide-linked subunits, HA_1 and HA_2 (Gething et al., 1986). Upon acidification, the initial step of the fusion cascade is a conformational change of the HA ectodomain into a fusogenic conformation (White et al., 1983). Thereby the N-terminus of the HA_2 subunit, the fusion sequence, is exposed toward the target membrane. Exposure of the fusion peptide after acidification occurs in a very short time span compared with the rate-limiting processes of fusion pore formation (White and Wilson, 1987; Stegmann et al., 1990; Pak et al., 1994; Krumbiegel et al., 1994). Therefore, we do not include this activation step into the model but consider all HA trimers to be in the active form from the onset of the pH drop. Lateral diffusion of activated HA trimers is modeled as a random walk from one unit cell into one of the four adjacent unit cells (left, right, up, or down).

R: receptor

An important step in HA-mediated cell fusion is the binding of HA to a sialic acid containing receptor of the target membrane (White et al., 1982). In erythrocytes this receptor is the transmembrane protein glycophorin. Similar to HA, lateral diffusion of receptors is modeled as a random walk from one unit cell into one of the four adjacent unit cells.

HA-R: HA-receptor contact

The formation of HA-receptor contacts is considered to be of importance in fusion in that the refolding of HA toward a fusion-competent conformation can be promoted by the interaction between HA1 and the sialic-acid-containing receptors (de Lima et al., 1995; Stegmann et al., 1995; Leikina et al., 2000). HA-R contacts are thought to be accomplished by weak noncovalent forces including hydrogen bonds (Sauter et al., 1992) and are thus fairly unstable. In the model, we describe the formation of the HA-receptor contacts as a reversible process that may take place if a HA trimer and a receptor molecule occupy unit cells that lie on top of each other. The HA trimer involved in the formation of a HA-receptor contact may be either freely diffusing or a member of an immobilized HA cluster (see below). The HA-R contact is considered immobile, though lateral movement of the involved partner molecules may continue after decay of the contact.

HA*: immobilized HA trimer captured in a HA cluster

The relevance of HA clusters for fusion was evidenced by several studies (Danieli et al., 1996; Blumenthal et al., 1996). The aggregation process is irreversible and driven by either adhesion of exposed hydrophobic sequences of the HA ectodomain (Burger et al., 1991; Korte and Herrmann, 1994) or by membrane curvature minimization (Kozlov and Chernomordik, 1998). In the model, HA aggregation occurs instantaneously whenever HA trimers occupy adjacent cells. Thus, aggregation includes the capture of a freely diffusing HA trimer by an adjacent HA intermediate (HA, HA aggregate, HA-R, or C; see below). With growing size, the lateral mobility of HA clusters decreases. Because no reliable experimental data exist on this immobilization, we consider HA clusters as completely immobilized. HA trimers belonging to a HA cluster are denoted by HA*.

C: HA-receptor-membrane link

A HA-R contact can make a transition to a stable, nonreversible link between HA and the target membrane, the HA-receptor-membrane link. It is reasonable to assume that this transition is associated with a transition of the activated HA trimer into an extended coiled-coil conformation and/or formation of an anti-parallel helices bundle (Bullough et al., 1994; Carr and Kim, 1993; Qiao et al., 1998; Shangguan et al., 1998; Skehel and Wiley, 1998) (see Discussion). In the model, formation of the stable HA-receptor-membrane link is described as an irreversible first-order reaction.

IP: ion-permissive early fusion pore

Formation of the early fusion pore starts with a small opening in the contact site that makes the inner lumen of the target cell continuous with that of the HA-expressing cells. This process leads to a change in the membrane potential of the target cell ($\Delta\psi$ signal), which can be measured by voltage-sensitive dyes (Blumenthal et al., 1996) and by capacitance patch-clamp techniques (Tse et al., 1993; Zimmerberg et al., 1994). We assume that the ion-permissive fusion pore consists of several HA-receptor contacts. Because the minimum number of membrane proteins required to form an opening is three, we define the early fusion pore as a cluster of HA-receptor contacts arranged in triangle configuration, i.e., occupying three adjacent unit cells in different rows or columns of the simulation lattice (cf. Fig. 1). As noted above, a HA-receptor contact may decay again into the constituting HA trimer and receptor. This implies that the ion-permissive fusion pore as defined in our model may decay as well. This kinetic instability is in line with the experimental observation of flickering $\Delta\psi$ signals in the early phase of fusion pore genesis (Melikyan et al., 1993; Spruce et al., 1991; Zimmerberg et al., 1994).

LP: lipid-permissive pore

The ion-permissive fusion pore may advance to a larger and more stable pore, the so-called lipid-permissive pore (also referred to as lipid-mixing pore) which can be monitored by lipid dye transfer between membranes ($\Delta\varphi$ signal). In the model, the transition IP→LP requires that at least three HA-receptor contacts of the early fusion pore arranged in triangle configuration transit into stable HA-receptor-membrane links (C). Hence, a lipid-permissive pore must comprise at least one cluster of three HA-receptor-membrane links arranged in triangle configuration (cf. Fig. 1).

Master equation

Let $p_{i,j}^{X}$ denote the probability to find a molecule of type X (X = HA, R, HA*, HA-R, or C) in the unit cell (i, j) at time t (the time argument will be dropped in the following). The subscripts i and j ($i, j = 1, \ldots, 50$) label the row and column of the simulation lattice. Generally, the time evolution of the probability is governed by the master equation:

$$\frac{\partial p_{i,j}^{X}}{\partial t} = \sum_{i',j'}\sum_{X'} A(i, j, X \leftarrow i', j', X') p_{i',j'}^{X'}$$
$$- \sum_{i',j'}\sum_{X'} A(i', j', X' \leftarrow i, j, X) p_{i,j}^{X} \qquad (2)$$

The linear time-evolution operator $A(i, j, X \leftarrow i', j', X')$ in Eq. 2 gives the probability with which occupation of the unit cell (i, j) by the molecular species X is affected by the molecular species X' resident in the unit cell (i', j'). Because the kinetic processes included in the model may take place either in a single cell (formation of HA-R or C) or between adjacent cells (lateral diffusion of HA, formation of HA* clusters) the summation across the cell indices i' and

j' in the master equation (Eq. 2) actually covers only $i' = i$, $i + 1$, $i - 1$ and $j' = j, j + 1, j - 1$. For example, occupation of the unit cell (i, j) by a mobile HA trimer may increase from 0 to 1 only due to invasion of a HA trimer from one of the neighboring unit cells or dissociation of a HA-receptor contact present in the same cell. Correspondingly, occupation of the unit cell (i, j) by a mobile HA trimer may decrease from 1 to 0 by transition of a HA trimer from this cell into one of the neighboring unit cells or by formation of HA-receptor contact within this cell (for rate constants refer to Table 1):

$$\frac{\partial}{\partial t} p_{i,j}^{HA} = k_{HA}[1 - p_{i,j}^{HA}][1 - p_{i,j}^{HA-R}][1 - p_{i,j}^{C}]$$

$$\times \left\{ \sum_{k=+1,-1} (p_{i+k,j}^{HA} + p_{i,j+k}^{HA}) \right\} + k_{-}p_{i,j}^{HA-R-}$$

$$- k_{HA}p_{i,j}^{HA} \sum_{k=+1,-1} ([1 - p_{i+k,j}^{HA}][1 - p_{i+k,j}^{HA-R}]$$

$$\times [1 - p_{i+k,j}^{C}] + [1 - p_{i,j+k}^{HA}][1 - p_{i,j+k}^{HA-R}]$$

$$\times [1 - p_{i,j+k}^{C}]) - k_{+}p_{i,j}^{HA}p_{i,j}^{R} \tag{3.1}$$

Similar equations hold for the time-dependent change of the probabilities for the other variables of the model:

$$\frac{\partial}{\partial t} p_{i,j}^{R} = k_{R}[1 - p_{i,j}^{R}][1 - p_{i,j}^{HA-R}][1 - p_{i,j}^{C}]$$

$$\times \left\{ \sum_{k=+1,-1} (p_{i+k,j}^{R} + p_{i,j+k}^{R}) \right\} + k_{-}p_{i,j}^{HA-R-}$$

$$- k_{R}p_{i,j}^{R} \sum_{k=+1,-1} ([1 - p_{i+k,j}^{R}][1 - p_{i+k,j}^{HA-R}]$$

$$\times [1 - p_{i+k,j}^{C}] + [1 - p_{i,j+k}^{R}][1 - p_{i,j+k}^{HA-R}]$$

$$\times [1 - p_{i,j+k}^{C}]) - k_{+}p_{i,j}^{HA}p_{i,j}^{R} \tag{3.2}$$

$$\frac{\partial}{\partial t} p_{i,j}^{HA-R} = k_{+}p_{i,j}^{HA}p_{i,j}^{R} - k_{-}p_{i,j}^{HA-R} \tag{3.3}$$

$$\frac{\partial}{\partial t} p_{i,j}^{C} = k_{c}p_{i,j}^{HA-R} \tag{3.4}$$

Simulation technique

Numerical solution of the master equation (Eq. 2) can be carried out by means of a compact and simple simulation algorithm (Gillespie, 1976).

1) Generating random initial occupations

At time 0, HA trimers and receptor molecules are randomly placed into the unit cells of the simulation lattice. This is performed by generating a random number $z \in [0, 1]$ for each unit cell of the lattice and putting a respective molecule into the cell if this random number is not larger than the given particle density. Such an algorithm assures random fluctuations of the initial molecule concentrations in the small simulation area.

2) Choosing a random time step

The probability p_{rest} that the distribution of the model variables across the simulation matrix does not change during the time interval Δt decreases exponentially; $p_{rest} = e^{-A_{tot}\Delta t}$. A_{tot} is the total transition probability obtained by adding up the transition probabilities of all possible elementary processes considered in the model. Thus, the time Δt required for any transition to occur is a stochastic quantity that can be computed by $\Delta t = -(1/A_{tot})\ln(z)$ with z being a uniformly distributed random number in [0,1]. The absolute time t is increased by the time step Δt, i.e., $t \rightarrow t + \Delta t$.

3) Selecting randomly a distinct transition process

The next step is to select from the whole set of all (N_{tot}) possible transition processes a single transition process to be executed within the time span Δt. To this end, one process out of all possible processes is selected. The probability of a process i to be chosen corresponds to its relative transition probability A_i/A_{tot}.

4) Updating the occupation numbers of the unit cells

Depending on the single transition process chosen, the occupation numbers of the involved unit cells have to be updated. If, for example, the selected transition process consists in the formation of a HA-R contact in the unit cell (i, j), new occupation numbers are obtained by putting $N_{i,j}^{HA} \rightarrow N_{i,j}^{HA} - 1$, $N_{i,j}^{R} \rightarrow N_{i,j}^{R} - 1$, $N_{i,j}^{HA-R} \rightarrow N_{i,j}^{HA-R} + 1$. $N_{i,j}^{X}$ denotes the occupation (0 or 1) of the unit cell (i, j) by the molecular species X.

Steps 2–4 of the simulation procedure are repeatedly executed until at least one ion-permissive pore and one lipid-permissive pore (for definitions see above) have emerged or, alternatively, until all HA trimers and receptors are trapped into isolated HA-receptor-membrane links that make the formation of an ion-permissive pore or a lipid-permissive pore impossible.

Stochastic simulations of single-cell fusion kinetics

The master-equation approach outlined above provides values for the stochastic variables t_{IP}^{sample} and t_{LP}^{sample} representing the delay times for the first occurrence of an ion-permissive fusion pore and of a lipid-permissive pore in the simulation lattice. Repeating the stochastic simulation for a

TABLE 1 Kinetic parameters used in simulations

	Model parameter	Value
Derived from measured values	HA density*	$750\ \mu m^{-2}$
	Receptor density[†]	$750\ \mu m^{-2}$
	HA diffusion rate (k_{HA})[‡]	$830\ s^{-1}$ (corresponding to a lateral diffusion coefficient of $3 \times 10^{-10}\ cm^2 s^{-1}$)
	Receptor diffusion rate (k_R)[§]	$83\ s^{-1}$ (corresponding to a lateral diffusion coefficient of $3 \times 10^{-11}\ cm^2 s^{-1}$)
Value estimated by adjustment of simulations to experimental data	Association rate (k_+) for the formation of an HA-R contact: HA + R → HA-R	$0.2\ s^{-1}$
	Association rate (k_-) for the decay of an HA-R contact: HA-R → HA + R	$0.15\ s^{-1}$
	Rate (k_C) for the formation of a tight HA-receptor-membrane link	$0.15\ s^{-1}$

*Approximate density of mobile HA trimers in the plasma membrane of the HA-expressing fibroblast cell lines (Danieli et al., 1996).
[†]Approximate density of the major sialic-acid-containing glycoprotein of red blood cells (glycophorin A with 2×10^5 copies per cell and a cell surface area of $150\ \mu m^2$).
[‡]Danieli et al., 1996; Gutman et al., 1993.
[§]See Sheetz, 1983.

sufficiently large number (N_{sample}) of independent simulation lattices one may generate sets of stochastic delay times, $\{t_{IP}^{sample,n}\}$ and $\{t_{LP}^{sample,n}\}$, $n = 1, \ldots, N_{sample}$, to derive cumulative frequency distributions:

$$F_{sample}^{IP}(t) = \frac{1}{N_{sample}} \sum_n \Theta\ (t - t_{IP}^{sample_n}) \qquad (3)$$

$$F_{sample}^{LP}(t) = \frac{1}{N_{sample}} \sum_n \Theta\ (t - t_{LP}^{sample_n}), \qquad (4)$$

whereby $\Theta(x)$ denotes the unit-step function; i.e., $\Theta(x) = 1$ if $x \geq 0$ (0 else). By employing Eq. 1, these cumulative frequency distributions for the first occurrence of a fusion-pore intermediate (ion-permissive pore or lipid-permissive pore) on the simulation lattice can be used to calculate the related cumulated frequency distributions $F_{tot}^{IP}(t)$ and $F_{tot}^{LP}(t)$ for the total effective contact area.

Stochastic simulations of fusion kinetics in cell suspensions

The cumulative distributions $F_{tot}^{IP}(t)$ and $F_{tot}^{LP}(t)$ count the frequency (or probability) for a fusion intermediate to occur in a single-cell fusion experiment within the time span t after initiation of the fusion process. These distributions can be used to provide large sets of stochastic delay times, $t_{IP}^{cell,i}$ and $t_{LP}^{cell,i}$, for the occurrence of an early fusion pore or a lipid-permissive pore in the ν-th cell-cell contact. Given that each lipid-permissive pore initiates lipid mixing, the overall dequenching signal (FDQ) ob-

served in a population of cells (N_{cells}) at time t represents the superposition of dequenching signals initiated at time $t_{LP}^{cell,i}$ by the ν-th cell pair:

$$FDQ_{population}(t) = \sum_{\nu=1}^{N_{cells}} FDQ_{single}(t; t_{LP}^{cell_\nu}) \qquad (5)$$

The time course for fluorescence dequenching due to formation of a lipid-permissive pore between a single pair of fusing cells at time t_0 can be roughly described by the function

$$FDQ_{single}(t; t_0) = \Theta(t - t_0)\left[1 - \exp\left(-\frac{t - t_0}{\tau}\right)\right], \quad (6)$$

where τ characterizes the kinetics of the lipid redistribution (Chen et al., 1993). Hence, the overall dequenching signal can be written as

$$FDQ_{population}(t) = \sum_{\nu=1}^{N_{cells}} \Theta(t - t_{LP}^{cell_\nu})\left[1 - \exp\left(-\frac{t - t_{LP}^{cell_\nu}}{\tau}\right)\right].$$
$$(7)$$

RESULTS

Simulation of single-cell fusion kinetics

The proposed mathematical model was first applied to simulate single-cell fusion kinetics as measured by Blumenthal et al. (1996). The numerical values of the kinetic parameters used in these simulations are depicted in Table 1. The rate
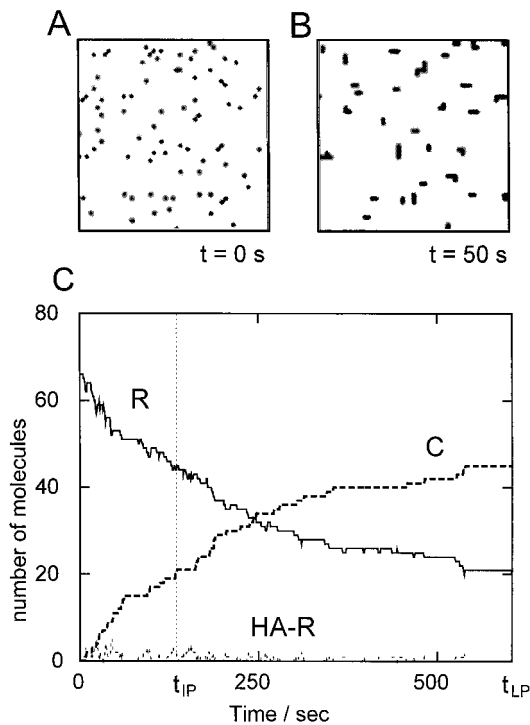
FIGURE 2 Simulation results for a 50×50 simulation lattice. (A) Example of the initial distribution of HA trimers across the simulation lattice. (B) Distribution of HA trimers across this simulation lattice after $t = 50$ s. Most of the HA molecules are trapped into immobile HA clusters. HA aggregation does not affect interactions with receptor molecules; i.e., HA trimers trapped into a cluster may still form weak HA-R contacts and stable HA-receptor-membrane links. (C) Example of stochastic trajectories for free receptors (R), HA-R contacts, and stable HA-receptor-membrane links (C). The vertical lines indicate the delay time $t_{IP} = 134$ s for the first occurrence of an ion-permissive pore ($\Delta\psi$ signal) and $t_{LP} = 605$ s for the first occurrence of a lipid-permissive pore ($\Delta\varphi$ signal) during the simulation.

constants for the diffusion of HA trimers and receptor molecules were calculated from measured diffusion coefficients D (Danieli et al., 1996; Gutman et al., 1993) according to $D = \Delta x^2/4t$, yielding $k = 4D/\Delta x^2$ with $\Delta x = 6$ nm for the rate with which a transition takes place from one unit cell to the neighboring unit cell. Numerical values for the remaining three rate constants were chosen such that a reasonable concordance between simulated and observed data was achieved. Note that the definition of the rate constants used in the model is different from the definition of phenomenological rate constants in chemical reaction kinetics in that the latter also include the collision probability (cross section).

Fig. 2, *A* and *B*, depict the distribution of HA trimers across the simulation lattice at the beginning ($t = 0$ s) and after 50 s of simulation. Placing the HA trimers randomly to the cells of the simulation lattice at $t = 0$ s, most of them are isolated without forming clusters with adjacent HA trimers. During the fusion process almost all HA trimers are trapped

into immobile HA-clusters of different shape. It has to be noted that irrespective of this clustering, the HA trimers keep interacting with receptor molecules to form HA-R contacts and HA-receptor-membrane links (not shown in Fig. 2, *A* and *B*).

Fig. 2 *C* shows an example of the time-dependent stochastic trajectories for free receptors, HA-R contacts, and stable HA-receptor-membrane links for one simulation on a 50×50 lattice. There is a decline in the number of free receptors from initially 65 molecules to ~20 molecules after 600 s. This decline is paralleled by a increase in the number of stable HA-receptor-membrane links hosting most of the available receptors because the number of HA-R contacts remains very small during the whole time course. The reversibility in the formation and decay of HA-R contacts is reflected by large fluctuations of the respective trajectory. The vertical lines in Fig. 2 *C* indicate the delay time $t_{ip} = 134$ s for the first occurrence of an ion-permissive pore ($\Delta\psi$ signal) and $t_{lp} = 605$ s for the first occurrence of a lipid-permissive pore ($\Delta\varphi$ signal) during the simulation.

From repeated simulations on a 50×50 simulation lattice we constructed the statistical distributions (Eqs. 3 and 4) of the characteristic time span needed for the first occurrence of an ion-permissive pore and of a lipid-permissive pore in a simulation lattice. Next, the respective distributions for the total contact area were computed by Eq. 1 using $N = 12$, i.e., considering the contact area to be constituted by 12 contact sites. The obtained theoretical distributions of $\Delta\psi$ signals (first occurrence of an ion-permissive pore) and $\Delta\varphi$ signals (first occurrence of a lipid-permissive pore) are both in reasonable concordance with the measurements (Fig. 3). It is seen, however, that the calculated cumulative distribution of $\Delta\psi$ signals exhibits a slightly steeper ascent than indicated by the measurements. This slight but systematic discrepancy could be possibly attributed to the choice of the number of contact sites, N, and the minimum number of HA trimers involved in the pore formation (see Discussion).

Variation of hemagglutinin and receptor densities

In a second series of simulations we studied the effect of varying concentrations of HA trimers and receptor molecules on the distribution of the delay times t_{IP} and t_{LP} for the first occurrence of an ion-permissive pore and a lipid-permissive pore (Fig. 4, *A–D*). The average occupation of the simulation lattice by HA trimers and receptor molecules was varied between 1% and 12%, which corresponds to actual molecule densities per membrane area of 250–3000 molecules/μm^2. As expected, the time delay in the formation of fusion intermediates becomes shorter with increasing concentrations of HA trimers and receptor molecules. According to our simulations, increasing the receptor density should be slightly more efficient in accelerating the fusion process than a comparable increase in HA density.
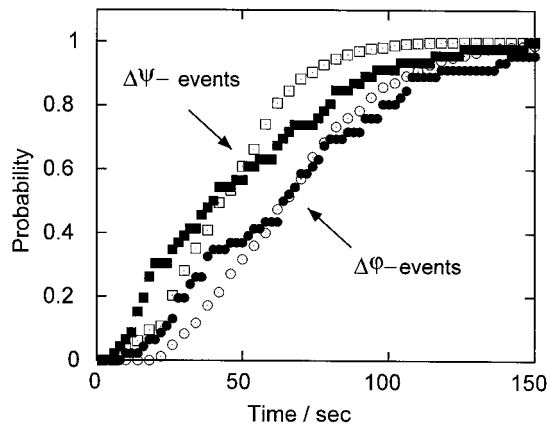
FIGURE 3 Kinetics of single-cell fusion: cumulative distribution of delay times for $\Delta\psi$ signals (first occurrence of an ion-permissive pore) and $\Delta\varphi$ signals (first occurrence of a lipid-permissive pore). Closed symbols refer to the experimental data of Blumenthal et al. (1996). Open symbols denote the simulated distributions based on the kinetic parameters in Table 1. The theoretical distributions have been obtained for a relative HA and receptor density of 3% occupation of the simulation lattice corresponding to 750 molecules per μm^2 of membrane area. The construction of the cumulative distributions is based on a total of 674 simulation trials on the simulation lattice. Only those signals have been taken into account that took place within a total simulation interval of 3000 s on a lattice.

Simulation of fusion signals observed in cell suspensions

A standard technique to trace the time-dependent formation of lipid-permissive pores ($\Delta\varphi$ signal) in cell suspensions consists in monitoring the fluorescence dequenching associated with the inter-membrane redistribution of a lipid dye. As outlined above (cf. Eq. 7) the dequenching signal at time
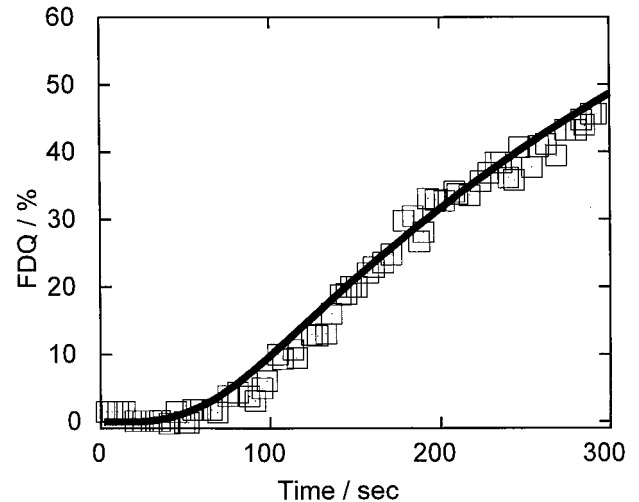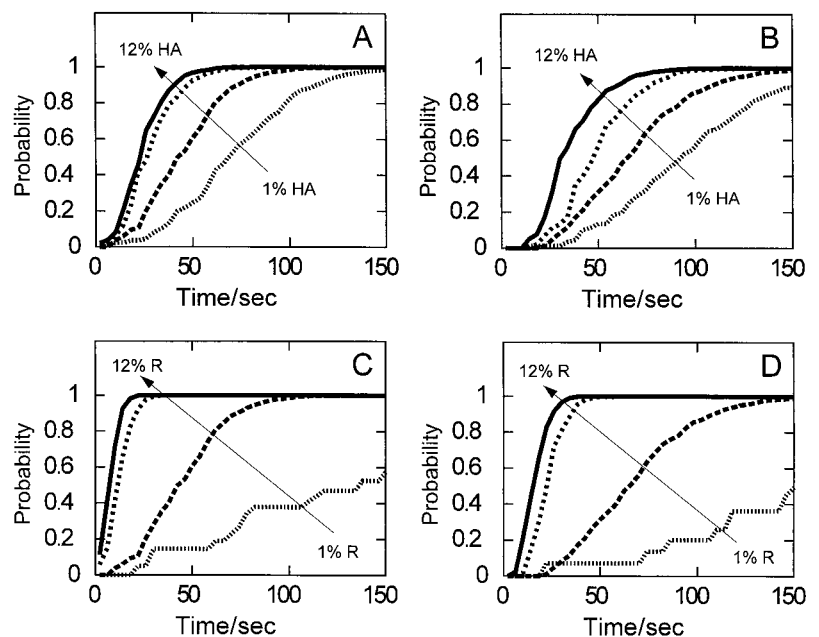

FIGURE 5 Kinetics of lipid mixing ($\Delta\varphi$ signal) in suspensions of fusing cells. The open squares refer to the fluorescence dequenching in suspensions of HA-expressing cells and red blood cells at 28–29°C measured by Danieli et al. (1996; see Fig. 3 of this paper). The solid line was obtained on the basis of Eq. 7 using the simulated distribution of delay times t_{LP} for the first occurrence of a lipid-permissive pore shown in Fig. 3. The rate constant for the kinetics of lipid redistribution was set to $\tau = 350$ s.

t represents a superposition of signals initiated at different times determined by stochastically distributed cell-cell fusion events. Fig. 5 shows a typical time course of $\Delta\varphi$ monitored during fusion between HA-expressing fibroblasts and red blood cells (see Fig. 3 of Danieli et al., 1996). The simulated time course in Fig. 5 was obtained according to Eq. 7 by applying the cumulative distribution of delay times t_{LP} for the first occurrence of a lipid-permissive pore ob-

FIGURE 4 Kinetics of single-cell fusion: influence of varying HA densities (*A* and *B*) and receptor densities (*C* and *D*) on the cumulative distribution of delay times for $\Delta\psi$ signals (first occurrence of an ion-permissive pore (*A* and *C*)) and $\Delta\varphi$ signals (first occurrence of a lipid-permissive pore (*B* and *D*)). The cumulative distributions have been calculated at relative HA and receptor densities of 1%, 3%, 9%, and 12% occupation of the simulation lattice corresponding to 250, 750, 2250, and 3000 molecules per μm^2 of membrane area. More than 600 simulations contribute to each curve.
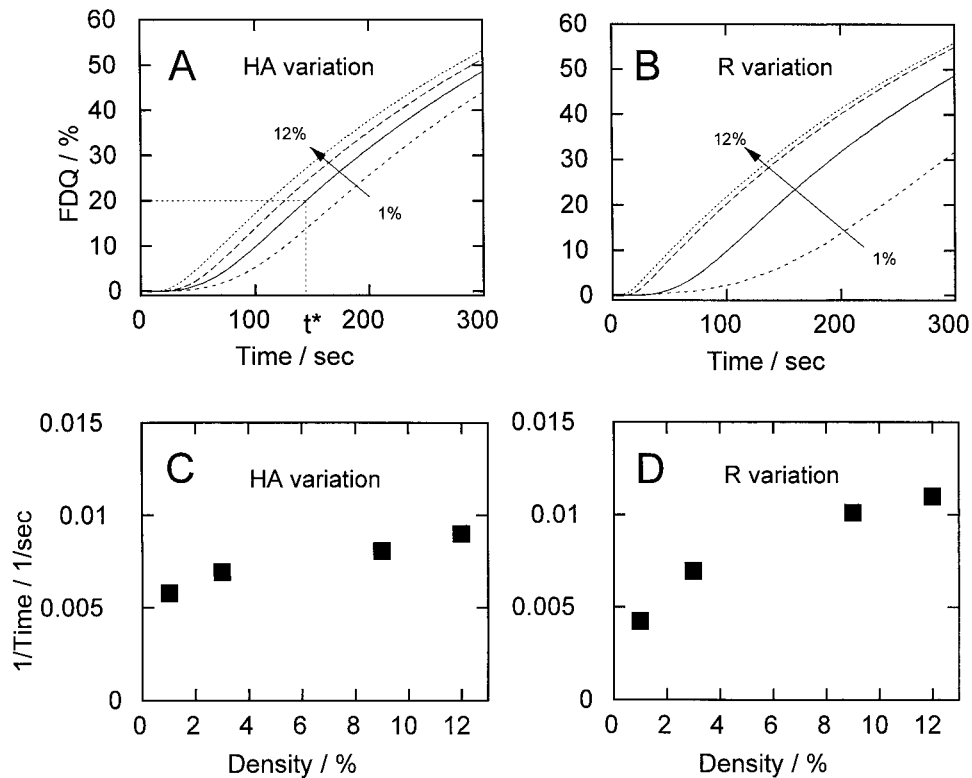
FIGURE 6 Influence of varying HA and receptor densities on the kinetics of lipid mixing ($\Delta\varphi$ signal) in suspensions of fusing cells. (*A* and *B*) The time courses have been calculated on the basis of Eq. 7 using the simulated distribution of delay times t_{LP} obtained at relative HA and receptor densities of 1%, 3%, 9%, and 12% occupation of the simulation lattice corresponding to 250, 750, 2250, and 3000 molecules per μm^2 of membrane area. The lag time t^* is defined as the time at which 20% of the FDQ signal has occurred. (*C* and *D*) Plot of the inverse lag time ($1/t^*$) at four different densities of HA trimers and receptors.

tained in the simulations of single-cell fusion events outlined above. The best fit to the experimental data was obtained by putting the rate constant for the kinetics of the lipid redistribution to the value $\tau = 350$ s. The excellent concordance between the simulated and measured time course of $\Delta\varphi$ demonstrates that the results obtained in the simulations of single-cell fusion events are fully consistent with kinetic data obtained in cell suspensions.

Based on the results shown in Fig. 4, we also simulated the influence of varying HA and receptor densities on the dequenching ($\Delta\varphi$) signal in cell suspensions (Fig. 6). The average occupation of the simulation lattice by HA trimers and receptor molecules was chosen to 1%, 3%, 9%, and 12% corresponding to actual molecule densities per membrane area between 250 and 3000 molecules/μm^2. As a measure for the lag period seen between initiation of fusion pore formation by acidification and notable increase of FDQ, we determined from the simulated time courses the time t^* at which 20% of the FDQ signal had occurred. Plotting the inverse lag time as a function of HA or receptor density indicates saturation with increasing densities (Fig. 6, *C* and *D*). The relative shortening of the lag period achieved by increasing the density of HA trimers from 1% to 12% is

~1.8. This value is of the same order as reported by Danieli et al. (1996) who have varied the HA content in the membrane by using different HA-expressing cell lines. Remarkably, our simulations predict a more significant decrease in the lag time (about three-fold) when increasing the density of receptors in the same range (1% to 12%) as the HA trimers.

DISCUSSION

To simulate the HA-mediated formation of a fusion pore we have developed a mathematical model that explicitly takes into account the stochastic nature of the molecular events underlying the fusion process. The proposed model encompasses the following steps reported in the literature to be included in fusion pore kinetics: 1) lateral diffusion and self-aggregation of the fusogenic viral membrane protein oligomers (trimers), 2) lateral diffusion of the receptor molecule in the target membrane, 3) formation of noncovalent contacts between HA trimers and receptors, 4) irreversible conversion of these contacts into tight links between HA and the target membrane, and 5) clustering of HA-receptor

contacts and HA-receptor-membrane links leading to the formation of early states of the fusion pore characterized by ion conductivity and a lipid flow between fusing cells, respectively.

A particular advantage of our approach is the possibility to model fusion signals measured in cell suspensions as a superposition of stochastic fusion signals arising from single-cell fusion events. This is the first successful attempt to model consistently both types of fusion kinetics. The fact that both types of experiments could be reasonably well described by choosing appropriate values for only three adjustable kinetic parameters (k_+, k_-, and k_C) underlines the reliability of the proposed model.

Validating the model

The contact site was assumed to be a lattice of small squared membrane units (6×6 nm) corresponding to a size of 300×300 nm. This is of the same order as the contact size between HA-containing liposomes deduced from quick-freezing electron microscopy (see Fig. 11f in Kanaseki et al., 1997). Furthermore, from electron microscopy images of Frolov et al. (2000) it can be roughly estimated that the radius of the membrane surface area involved in the formation of direct contacts between erythrocytes and HA-expressing cells is on the order of 100–150 nm. Due to the larger size of attachment area between fusing cells (Danieli et al., 1996; Frolov et al., 2000) the existence of several contact sites is a reasonable assumption.

Numerical values for the kinetic parameters of the model have been either taken from the literature or estimated by comparing simulation results with experimental data. A value of ~3 mM was estimated for the dissociation constant of the sialic acid-HA ectodomain complex (Sauter et al., 1992). Based on this value it was concluded that on the average the percentage of HA trimers and receptors temporarily involved in HA-R contacts should be lying in the range 60% to 98% (Leikina et al., 2000). This estimate is in good agreement with our theoretical finding that for a lattice occupation of 3% HA trimers and 3% receptor molecules (corresponding to a normal membrane density of 750 molecules/μm^2) the percentage of HA trimers and receptors involved in HA-R contacts was ~53% during the initial phase of the stochastic simulations.

The existence of an early fusion pore was evidenced by cell membrane capacitance measurements and by lipid dyes sensitive to the membrane potential (Blumenthal et al., 1996; Zimmerberg et al., 1994; Tse et al., 1993). In the model, an early fusion pore is defined as a cluster of three HA-R contacts in triangle configuration. Based on this assumption the model provides a satisfactory statistical distribution of single-cell $\Delta\psi$ signals. Nevertheless, it cannot be excluded that the number of HA-R contacts constituting an early fusion pore is different from three (see below).

In the model, formation of HA-R contacts is described as a reversible process. Hence, ion-permissive pores may decay again. In the simulations this is reflected by random fluctuations in the number of early fusion pores. Such instability of the ion-permissive pore was indeed elucidated by a flickering of its conductance (Melikyan et al., 1993; Spruce et al., 1991; Zimmerberg et al., 1994). A further important consequence implied by the possible decay of HA-R contacts is that the first lipid-permissive pore (defined as a cluster of stable HA-R cross-links) does not necessarily emerge from the first early fusion pore.

Experimental studies have shown that the essential conformational change of HA into a fusion-competent state is supported by HA-receptor interactions (de Lima et al., 1995; Stegmann et al., 1995; Leikina et al., 2000). To describe adequately this observation, in the model, formation of a stable HA-receptor-membrane link proceeds obligatorily via a reversible HA-R contact; i.e., there is no direct transition HA + R $\rightarrow$ C. The nature of this essential conformation change of activated HA has still to be identified. Following recent studies one may suggest that this transformation reflects later stages of the refolding of HA. For example, this transition might be accompanied by the formation of the extended coiled-coil motif and/or of an anti-parallel helices bundle (Bullough et al., 1994; Chen et al., 1999) facilitating or mediating the close approach of membranes necessary to form a stable fusion pore. The estimated half-time value for the transition rate HA-R $\rightarrow$ C amounts to ~5 s ($\ln2/k_p$). In our model, the transition rate refers to the conformational change. Of course, the time required for formation of the first ion-permissive pore is much longer. Bentz (2000) found a rate of 10^4 s in his kinetic fusion model as the characteristic time required for the conformational change to occur after triggering of the fusion process. This value includes all processes preceding the conformational change, for example, aggregation of HA trimers and formation of HA-receptor contacts, which in our model are considered separately.

The lipid-permissive pore is commonly regarded as an important intermediate of fusion pore formation. In the model, the lipid-permissive pore requires three HA trimers arranged in triangle geometry. This assumption was essentially based on experimental observations of Danieli et al. (1996) who concluded that membrane fusion requires the concerted action of at least three activated HA trimers. In contrast, Blumenthal et al. (1996) interpreted their experiments on the basis of a theoretical model that yielded about six HA trimers to be necessary for fusion. It has to be considered that the latter estimate was derived from kinetic data on the formation of solute-permissive fusion pores, whereas Danieli et al. (1996) derived their estimate from measurements of lipid mixing. We have not studied in detail how changes in the assumption on the minimum configuration of an ion-permissive pore and a lipid-permissive pore

may affect the quality of the simulations with respect to available experimental data.

Aggregation of HA trimers to larger clusters is thought to be caused by interactions of hydrophobic sequences of the HA trimer. It has been concluded that apart from the N-terminus of the HA ectodomain other hydrophobic sequences become also exposed after activation of HA by the low-pH trigger (Korte and Herrmann, 1994; Burger et al., 1991). A rapid and irreversible aggregation of HA on cells is consistent with experimental data (Ellens et al., 1990; Melikyan et al., 1995a; Danieli et al., 1996; Gutman et al., 1993). From photobleaching experiments, it was concluded that aggregation of HA trimers results in a suppression of fusion (Gutman et al., 1993). In the model, HA aggregates are treated as completely immobilized but without becoming inactivated, i.e., without losing their competence to interact with receptors and to form stable HA-receptor contacts. This is a reasonable assumption, keeping in mind that the experimental data that served as the basis for comparison with the model are based on HA-expressing cells from the influenza virus A Japan strain (Danieli et al., 1996; Blumenthal et al., 1996). It has been shown that inactivation of HA from the Japan strain of influenza virus (A/Japan/305/57) is a very slow process (Puri et al., 1990; Korte et al., 1999). Moreover, neglecting HA inactivation as a kinetic relevant process in a contact site seems to be justified by the observation that HA inactivation is suppressed in the presence of the target membrane (Ramalhosantos et al., 1993; Leikina et al., 2000).

Simulation of single-cell fusion kinetics

In our simulations of single-cell fusion kinetics we could achieve a good overall concordance with the experimental data of Blumenthal et al. (1996). Nevertheless, the computed cumulative distributions for the first occurrence of $\Delta\psi$ signals appear to be slightly steeper than the corresponding experimental distributions. This discrepancy can be possibly accounted for by the fact that we used a fixed number of $N = 12$ simulation lattices of size to represent the effective contact area (1 μm^2) between fusing cells. Actually, the size of the contact area itself is a stochastic variable so that the number N of simulation lattices and hence the shape of the cumulative distribution calculated on the basis of Eq. 1 will vary from one single-cell complex to the other. Thus, the relative contact area, i.e., the membrane fraction actually involved in the formation of inter-membrane contacts, turns out to be an essential parameter of the model.

The rate of fusion pore formation depends on HA and receptor density

The model allows us to address the influence of distinct parameters on the fusion kinetics. For example, from ex-

periments, opposite conclusions were drawn on the role of the HA-receptor interactions in fusion. Alford et al. (1994) observed a decline of influenza virus fusion at high concentrations of sialic-acid-bearing gangliosides in the liposomal target. They concluded that only those HA trimers can form a fusion pore that are not associated with receptors of the target membrane (see also Ellens et al., 1990). Here, simulating the effect of increasing HA densities (at constant receptor density) we found a significant increase in the overall rate of the fusion process. This result is in agreement with experimental findings (Danieli et al., 1996; Clague et al., 1991). Similarly, increasing the receptor density (at constant HA density), the model predicts an acceleration of the fusion process. Several independent studies arrived at the conclusion that HA-receptor complexes are important for cell fusion (see above).

Nevertheless, it is known that HA can trigger fusion of influenza viruses with lipid membranes bearing no receptor (Schoen et al., 1996). Thus, in principal, one has to consider that also HAs not associated with a receptor can be involved in triggering membrane fusion. Such a mechanism could be implemented in our approach. However, we did not include this mechanism for several reasons. First, our study is to our knowledge the first approach describing protein-mediated fusion as a stochastic process. To provide a clearly arranged model, we kept the number of processes/steps low. Second, a goal of our work was to develop a model applicable also to fusion of other viruses. Notably, for fusion of other enveloped viruses, e.g., human immunodeficiency virus, interaction with receptors is essential for fusion-mediating viral proteins to transform into their fusion-active conformation. Third, we consider the rather high part of HAs bound to receptors (see above) as a justification to neglect a fusion mediated by HAs not bound to receptors.

Simulation of fusion experiments with cell populations

Based on our stochastic approach we have simulated the kinetics of lipid mixing between fusing HA-expressing cells and red blood cells in suspension. The time course of lipid mixing can be represented as a convolution of two distinct kinetic processes (Chen et al., 1993): 1) initiation of lipid mixing due to the formation of a lipid-permissive pore, triggering 2) redistribution of the fluorescent lipid-like probe between the fusing membranes. The latter process can be monitored by fluorescence dequenching. Chen et al. (1993) have shown that lipid (probe) redistribution between two fusing cells joined by a narrow neck can be approximated by a single exponential (see Eq. 6) decaying with a characteristic time τ. Choosing a value $\tau = 350$ s for the rate constant of lipid redistribution we obtained a surprisingly good concordance of these simulations with (cuvette) experiments carried out at 28–29°C (Danieli et al., 1996). Chen et al. (1993) have developed a theoretical approach to

relate the parameter τ to the size (radius) of the two cells, the lateral diffusion coefficient of the probe, and the radius of the fusion pore. The size of the early fusion pore should be in the range 10–15 nm because the thickness of each bilayer is ~5 nm, and the inner diameter of the early fusion pore is ~4 nm (Kanaseki et al., 1997). The radius of the HA-expressing fibroblasts is ~11 μm (see Fig. 1 *A* in Danieli et al., 1996), and the radius of red blood cells is ~3 μm. Taking these values and a lateral diffusion coefficient of 0.5×10^{-8} μm^2/s for R18 (extrapolated from the value of 0.3×10^{-8} at 22°C (Aroeti and Henis, 1986), the formalism of Chen et al. (1993) yields $\tau = 420$ s, which is very close to the fitted value of $\tau = 350$ s.

In summary, our model provides a satisfactory quantitative simulation of kinetic data on HA-mediated fusion pore formation gathered by different types of kinetic measurements. Further progress in mathematical modeling will depend upon the availability of reliable kinetic data (rate constants) for the various elementary processes. If so, other steps and intermediates of the HA fusion process as, for example, the well established hemifusion intermediate (Kemble et al., 1993; Melikyan et al., 1995b; Nussler et al., 1997) can be integrated into simulation. Nevertheless, at the current state of experimental research, the proposed model appears to be consistent with most kinetic features of fusion pore formation documented in the literature. Finally it has to be pointed out that the proposed stochastic approach is also applicable to other types of membrane-membrane interactions such as, for example, cell-cell attachment.

REFERENCES

Alford, D., H. Ellens, and J. Bentz. 1994. Fusion of influenza virus with sialic acid-bearing target membranes. *Biochemistry*. 33:1977–1987.

Aroeti, B., and Y. I. Henis. 1986. Fusion of native virions with human erythrocytes. *Exp. Cell Res.* 170:322–337.

Baker, K. A., R. E. Dutch, R. A. Lamb, and T. S. Jardetzky. 1999. Structural basis for paramyxovirus-mediated membrane fusion. *Mol. Cell.* 3:309–319.

Bentz, J. 1992. Intermediates and kinetics of membrane fusion. *Biophys. J.* 63:448–459.

Bentz, J. 2000. Minimal aggregate size and minimal fusion unit for the first fusion pore of influenza hemagglutinin-mediated membrane fusion. *Biophys. J.* 78:227–245.

Blumenthal, R., D. P. Sarkar, S. Durell, D. E. Howard, and S. J. Morris. 1996. Dilation of the influenza hemagglutinin fusion pore revealed by the kinetics of individual cell-cell fusion events. *J. Cell Biol.* 135:63–71.

Böttcher, C., K. Ludwig, A. Herrmann, M. van Heel, and H. Stark. 1999. Structure of influenza haemagglutinin at neutral and at fusogenic pH by electron cryo-microscopy. *FEBS Lett.* 463:255–259.

Bullough, P. A., F. M. Hughson, J. J. Skehel, and D. C. Wiley. 1994. Structure of influenza haemagglutinin at the pH of membrane fusion. *Nature.* 371:37–43.

Burger, K. N. J., S. A. Wharton, R. A. Demel, and A. J. Verkleij. 1991. Interaction of influenza virus hemagglutinin with a lipid monolayer: a comparison of the surface activities of intact virions, isolated hemagglutinins and a synthetic fusion peptide. *Biochemistry.* 30:11173–11180.

Caffrey, M., M. L. Cai, J. Kaufman, S. J. Stahl, P. T. Wingfield, D. G. Covell, A. M. Gronenborn, and G. M. Clore. 1998. Three-dimensional solution structure of the 44 kDa ectodomain of SIV gp41. *EMBO J.* 17:4572–4584.

Carr, C. M., and P. S. Kim. 1993. A spring-loaded mechanism for the conformational change of influenza hemagglutinin. *Cell.* 73:823–832.

Chan, D. C., D. Fass, J. M. Berger, and P. S. Kim. 1997. Core structure of gp41 from the HIV envelope glycoprotein. *Cell.* 89:263–273.

Chen, Y. D., R. J. Rubin, and A. Szabo. 1993. Fluorescence dequenching kinetics of single cell-cell fusion complexes. *Biophys. J.* 65:325–333.

Chen, J., J. J. Skehel, and D. C. Wiley. 1999. N- and C-terminal residues combine in the fusion-pH influenza hemagglutinin HA$_2$ to form an N cap that terminates the triple-stranded coiled coil. *Proc. Natl. Acad. Sci. U.S.A.* 96:8967–8972.

Clague, M. J., C. Schoch, and R. Blumenthal. 1991. Delay time for influenza virus hemagglutinin-induced membrane fusion depends on hemagglutinin surface density. *J. Virol.* 65:2402–2407.

Danieli, T., S. L. Pelletier, Y. I. Henis, and J. M. White. 1996. Membrane fusion mediated by the influenza virus hemagglutinin requires the concerted action of at least three hemagglutinin trimers. *J. Cell Biol.* 133:559–569.

de Lima, M. C., D. Ramalho-Santos, V. A. Flasher, S. Slepushkin, S. Nir, and N. Duzgunes. 1995. Target cell membrane sialic acid modulates both binding and fusion activity of influenza virus. *Biochim. Biophys. Acta.* 1236:323–330.

Doms, R. W., and A. Helenius. 1986. Quaternary structure of influenza virus hemagglutinin after acid treatment. *J. Virol.* 60:833–839.

Durell, S. R., I. Martin, J. M. Ruysschaert, Y. Shai, and R. Blumenthal. 1997. What studies of fusion peptides tell us about viral envelope glycoprotein-mediated membrane fusion. *Mol. Membr. Biol.* 14:97–112.

Ellens, H., J. Bentz, F. Mason, F. Zhang, and J. M. White. 1990. Fusion of influenza hemagglutinin-expressing fibroblasts with glycophorin-bearing liposomes: role of hemagglutinin surface density. *Biochemistry.* 29:9697–9707.

Fass, D., S. C. Harrison, and P. S. Kim. 1996. Retrovirus envelope domain at 1.7 angstrom resolution. *Nat. Struct. Biol.* 3:465–469.

Frolov, V. A., M.-S. Cho, P. R. T. S. Bronk, and J. Zimmerberg. 2000. Multiple local contact sites are induced by GPI-linked influenza hemagglutinin during hemifusion and flickering pore formation. *Traffic.* 1:622–630.

Gething, M.-J., R. W. Doms, D. York, and J. White. 1986. Studies on the mechanism of membrane fusion: site-specific mutagenesis of the hemagglutinin of influenza virus. *J. Cell Biol.* 102:11–23.

Gillespie, D. T. 1976. A general method for numerically simulating the stochastic time evolution of coupled chemical reactions *J. Comp. Phys.* 22:403–434.

Gutman, O., T. Danieli, J. M. White, and Y. I. Henis. 1993. Effects of exposure to low pH on the lateral mobility of influenza hemagglutinin expressed at the cell surface: correlation between mobility inhibition and inactivation. *Biochemistry.* 32:101–106.

Kanaseki, T., K. Kawasaki, M. Murata, Y. Ikeuchi, and S. Ohnishi. 1997. Structural features of membrane fusion between influenza virus and liposome as revealed by quick-freezing electron microscopy. *J. Cell Biol.* 137:1041–1056.

Kemble, G. W., Y. I. Henis, and J. M. White. 1993. GPI-anchored and transmembrane-anchored influenza hemagglutinin differ in structure and receptor binding activity. *J. Cell Biol.* 122:1253–1265.

Kobe, B., R. J. Center, B. E. Kemp, and P. Poumbourios. 1999. Crystal structure of human T cell leukemia virus type 1 gp21 ectodomain crystallized as a maltose-binding protein chimera reveals structural evolution of retroviral transmembrane proteins. *Proc. Natl. Acad. Sci. U.S.A.* 96:4319–4324.

Korte, T., and A. Herrmann. 1994. pH-Dependent binding of the fluorophore bis-ANS to influenza virus reflects the conformational change of hemagglutinin. *Eur. Biophys. J.* 23:105–113.

Korte, T., K. Ludwig, F. P. Booy, R. Blumenthal, and A. Herrmann. 1999. Conformational intermediates and fusion activity of influenza virus hemagglutinin. *J. Virol.* 73:4567–4574.

Kozlov, M. M., and L. V. Chernomordik. 1998. A mechanism of protein-mediated fusion: coupling between refolding of the influenza hemagglutinin and lipid rearrangements. *Biophys. J.* 75:1384–1396.

Krumbiegel, M., A. Herrmann, and R. Blumenthal. 1994. Kinetics of the low pH-induced conformational changes and fusogenic activity of influenza hemagglutinin. *Biophys. J.* 67:2355–2360.

Leikina, E., I. Markovic, L. V. Chernomordik, and M. M. Kozlov. 2000. Delay of influenza hemagglutinin refolding into a fusion-competent conformation by receptor binding: a hypothesis. *Biophys. J.* 79: 1415–1427.

Ludwig, K., T. Korte, and A. Herrmann. 1995. Analysis of delay times of hemagglutinin-mediated fusion between influenza virus and cell membranes. *Eur. Biophys. J.* 24:55–64.

Malashkevich, V. N., B. J. Schneider, M. L. McNally, M. A. Milhollen, J. X. Pang, and P. S. Kim. 1999. Core structure of the envelope glycoprotein GP2 from Ebola virus at 1.9-angstrom resolution. *Proc. Natl. Acad. Sci. U.S.A.* 96:2662–2667.

Markovic, I., H. Pulyaeva, A. Sokoloff, and L. V. Chernomordik. 1998. Membrane fusion mediated by baculovirus gp64 involves assembly of stable gp64 trimers into multiprotein aggregates. *J. Cell Biol.* 143: 1155–1166.

Melikyan, G. B., W. D. Niles, and F. S. Cohen. 1993. Influenza virus hemagglutinin-induced cell-planar bilayer fusion: quantitative dissection of fusion pore kinetics into stages. *J. Gen. Physiol.* 102:1151–1170.

Melikyan, G. B., W. D. Niles, and F. S. Cohen. 1995a. The fusion kinetics of influenza hemagglutinin expressing cells to planar bilayer membranes is affected by HA density and host cell surface. *J. Gen. Physiol.* 106: 783–802.

Melikyan, G. B., J. M. White, and F. S. Cohen. 1995b. GPI-anchored influenza hemagglutinin induces hemifusion to both red blood cell and planar bilayer membranes. *J. Cell Biol.* 131:679–691.

Morris, M. B., D. P. Sarkar, J. M. White, and R. Blumenthal. 1989. Kinetics of pH-dependent fusion between 3t3 fibroblasts expressing influenza hemagglutinin and red blood cells. *J. Biol. Chem.* 264: 3972–3978.

Nussler, F., M. J. Clague, and A. Herrmann. 1997. Meta-stability of the hemifusion intermediate induced by glycosylphosphatidylinositol-anchored influenza hemagglutinin. *Biophys. J.* 73:2280–2291.

Pak, C. C., M. Krumbiegel, and R. Blumenthal. 1994. Intermediates in influenza virus Pr/8 haemagglutinin-induced membrane fusion. *J. Gen. Virol.* 75:395–399.

Puri, A., F. P. Booy, R. W. Doms, J. M. White, and R. Blumenthal. 1990. Conformational changes and fusion activity of influenca virus hemagglutinin of the H2 and H3 subtypes: effects of acid pretreatment. *J. Virol.* 64:10108–10113.

Qiao, H., S. L. Pelletier, L. Hoffman, J. Hacker, R. T. Armstrong, and J. M. White. 1998. Specific single or double proline substitutions in the "spring-loaded" coiled-coil region of the influenza hemagglutinin impair or abolish membrane fusion activity. *J. Cell Biol.* 141:1335–1347.

Ramalhosantos, J., S. Nir, N. Duzgunes, A. P. Decarvalho, and M. D. P. Delima. 1993. A common mechanism for influenza virus fusion activity and inactivation. *Biochemistry.* 32:2771–2779.

Sauter, N. K., J. E. Hanson, G. D. Glick, J. H. Brown, R. L. Crowther, S.-J. Park, J. J. Skehel, and D. C. Wiley. 1992. Binding of influenza virus hemagglutinin to analogs of its cell-surface receptor, sialic acid: analysis by proton nuclear magnetic resonance spectroscopy and x-ray crystallography. *Biochemistry.* 31:9609–9621.

Schoen, P., L. Leserman, and J. Wilschut. 1996. Fusion of reconstituted influenza virus envelopes with liposomes mediated by streptavidin/biotin interactions. *FEBS Lett.* 390:315–318

Shangguan, T., D. P. Siegel, J. D. Lear, D. Axelsen, D. Alford, and J. Bentz. 1998. Morphological changes and fusogenic activity of influenza virus hemagglutinin. *Biophys. J.* 74:54–62.

Sheetz, M. P. 1983. Membrane skeletal dynamics: role in modulation of red cell deformability of transmembrane proteins, and shape. *Semin. Hematol.* 20:175–188.

Skehel, J. J., and D. C. Wiley. 1998. Coiled coils in both intracellular vesicle and viral membrane fusion. *Cell.* 95:871–874.

Spruce, A. E., A. Iwata, and W. Almers. 1991. The first milliseconds of the pore formed by a fusogenic viral envelope protein during membrane fusion. *Proc. Natl. Acad. Sci. U.S.A.* 88:3623–3627.

Stegmann, T., I. Bartoldus, and J. Zumbrunn. 1995. Influenza hemagglutinin-mediated membrane fusion: influence of receptor binding on the lag phase preceding fusion. *Biochemistry.* 34:1825–1832.

Stegmann, T., J. M. White, and A. Helenius. 1990. Intermediates in influenza induced membrane fusion. *EMBO J.* 9:4231–4241.

Tan, K. M., J. H. Liu, J. H. Wang, S. Shen, and M. Lu. 1997. Atomic structure of a thermostable subdomain of HIV-1 gp41. *Proc. Natl. Acad. Sci. U.S.A.* 94:12303–12308.

Träuble, J., and E. Sackmann. 1972. Studies of the crystalline-liquid crystalline phase transition of lipid model membranes. III. Structure of a steroid-lecithin system below and above the lipid-phase transition. *J. Am. Chem. Soc.* 94:4499–4510.

Tse, F. W., A. Iwata, and W. Almers. 1993. Membrane flux through the pore formed by a fusogenic viral envelope protein during cell fusion. *J. Cell Biol.* 121:543–552.

Weissenhorn, W., A. Carfi, K. H. Lee, J. J. Skehel, and D. C. Wiley. 1998. Crystal structure of the Ebola virus membrane fusion subunit, GP2, from the envelope glycoprotein ectodomain. *Mol. Cell.* 2:605–616.

Weissenhorn, W., A. Dessen, S. C. Harrison, J. J. Skehel, and D. C. Wiley. 1997. Atomic structure of the ectodomain from HIV-1 gp41. *Nature.* 387:426–430.

White, J. M., and I. A. Wilson. 1987. Anti-peptide antibodies detect steps in a protein conformational change: low-ph activation of the influenza virus hemagglutinin. *J. Cell Biol.* 105:2887–2896.

White, J., A. Helenius, and M.-J. Gething. 1982. Haemagglutinin of influenza virus expressed from a cloned gene promotes membrane fusion . *Nature.* 300:658–659.

White, J., M. Kielian, and A. Helenius. 1983. Membrane fusion proteins of enveloped animal viruses. *Q. Rev. Biophys.* 16:151–195.

Wilson, I. A., J. J. Skehel, and D. C. Wiley. 1981. Structure of the haemagglutinin membrane glycoprotein of influenza virus at 3 Å resolution. *Nature.* 289:366–373.

Zimmerberg, J., R. Blumenthal, D. P. Sarkar, M. Curran, and S. J. Morris. 1994. Restricted movement of lipid and aqueous dyes through pores formed by influenza hemagglutinin during cell fusion. *J. Cell Biol.* 127:1885–1894.